Modification of palladium surfaces by bismuth adatoms or clusters: Effect on electrochemical activity and selectivity towards polyol electrooxidation

ARTICLE *in* INTERNATIONAL JOURNAL OF HYDROGEN ENERGY · APRIL 2014

Impact Factor: 3.31 · DOI: 10.1016/j.ijhydene.2014.03.076

INTERNATIONAL JOURNAL OF HYDROGEN ENERGY 39 (2014) 15877–15886

Available online at www.sciencedirect.com

ScienceDirect

journal homepage: www.elsevier.com/locate/he

Modification of palladium surfaces by bismuth adatoms or clusters: Effect on electrochemical activity and selectivity towards polyol electrooxidation

C. Coutanceau*, A. Zalineeva, S. Baranton, M. Simoes

Université de Poitiers, IC2MP, Equipe «Catalyse et Milieux Non-Conventionnels», UMR CNRS 7285, 4 rue Michel brunet, 86022 Poitiers, France

ARTICLE INFO

Article history:
Received 30 August 2013
Received in revised form
10 March 2014
Accepted 13 March 2014
Available online 13 April 2014

Keywords:
Adatoms
Bismuth
Clusters
Glycerol
Oxidation
Palladium

ABSTRACT

The syntheses of Bi-modified Pd catalysts with a controlled size distribution are presented as well as the characterizations of their structures and of their surfaces. Effects of the modification either of non-supported Pd nanospheres by spontaneous deposition of Bi or of carbon-supported Pd-based nanomaterials by decoration with bismuth clusters on the electrocatalytic activity towards glycerol electrooxidation were evaluated and compared in alkaline medium. The method of bismuth deposition has a dramatic effect on the activity of the palladium based catalysts: spontaneous deposition of Bi on non-supported Pd nanoparticles leads to relatively low activity enhancement, whereas decoration of carbon-supported Pd nanoparticles by Bi_2O_3 and $Bi(OH)_3$ clusters leads to very high activity increase at low overpotentials. *In situ* infrared spectroscopy indicated that the modification of Pd by Bi did not affect the selectivity of glycerol oxidation, whereas in the case of Pt containing catalyst, a dramatic change in selectivity occurred at low potentials.

Introduction

The recent environmental and energy challenges faced by society could be addressed by envisaging the production of electricity using hydrogen/air solid polymer electrolyte fuel cells (SPEFC). However hydrogen, which is the most abundant element in the universe, does not exist as dihydrogen molecule on earth, but is mainly combined with carbon (hydrocarbon) or oxygen (water), so that molecular hydrogen has to be produced. The most common method for hydrogen production consists in the reforming of fossil hydrocarbons. But the reforming process of such compounds, although less expensive than other hydrogen production methods, produces significant amount of carbon monoxide which is detrimental for the proton exchange membrane fuel cell (PEMFC) performances [1], so that complicated and costly hydrogen purification processes have to be implemented in parallel. Water electrolysis is also being developed, leading to high purity hydrogen, suitable to feed a low temperature fuel cell, such as a PEMFC or an alkaline fuel cell (AFC) [2–4]. In water electrolysis liquid or gaseous water is fed to the anodic

* *Corresponding author.*
E-mail address: christophe.coutanceau@univ-poitiers.fr (C. Coutanceau).
http://dx.doi.org/10.1016/j.ijhydene.2014.03.076

compartment where it is oxidized producing oxygen and protons:

$$H_2O \rightarrow 1/2O_2 + 2H^+ + 2e^- \quad (1)$$

Oxygen evolves in the gaseous phase, whereas the electrons circulate in the external circuit and protons cross-over the membrane, reaching the cathodic compartment where they are reduced by the electrons coming from the external circuit, thus producing hydrogen, as follows:

$$2H^+ + 2e^- \rightarrow H_2 \quad (2)$$

This corresponds to the overall decomposition of water into hydrogen and oxygen:

$$H_2O \rightarrow H_2 + 1/2O_2 \quad (3)$$

with $\Delta H = 286$ kJ and $\Delta G = 237$ kJ (mole H_2)$^{-1}$ under standard conditions.

The corresponding theoretical cell voltage can be calculated from ΔG, i.e. $E_{cell} = \Delta G/2F$, giving $E_{cell} = 1.23$ V. But the overvoltage of the oxygen evolution reaction (OER) is hardly decreased below 0.5 V (i.e. a cell voltage of at least 1.7–1.8 V at 1 A cm^{-2}) [5], so that the energy yield between both systems, water electrolysis and fuel cell, is lower than 40% (considering a H_2/air PEMFC performance of 1 A cm^{-2} at 0.7 V). An alternative can be the use of compounds produced from biomass as hydrogen source since the theoretical cell voltage for their electrochemical decomposition with hydrogen production is lower than the theoretical cell voltage of water electrolysis (1.23 V under standard conditions) [6,7]. For example, glycerol can be oxidized in the anodic compartment of the electrolysis cell instead of water, producing carbon dioxide and protons:

$$CH_2OH–CHOH–CH_2OH + 3H_2O \rightarrow 3CO_2 + 14H^+ + 14e^- \quad (4)$$

The protons are reduced to hydrogen in the cathodic compartment according to Eq. (2). The overall electrochemical decomposition reaction of glycerol into hydrogen and carbon dioxide is:

$$CH_2OH–CHOH–CH_2OH + 3H_2O \rightarrow 3\,CO_2 + 7H_2 \quad (5)$$

with $\Delta G_r = 3.9$ kJ mol$^{-1}{}_{glycerol}$, giving $E_{cell} = 0.003$ V [8].

The thermodynamic data point out that the use of alcohols, and particularly of glycerol, as anodic reactants in an electrolysis cell could be energetically more interesting than water for the production of hydrogen.

Despite their promising thermodynamics properties, the main limitation in using alcohols as hydrogen source in an electrolysis cell is the slow kinetics of their oxidation reaction. For this reason, alkaline medium has to be preferred to acid medium: the electrochemical reaction kinetics of fuel oxidation is faster [9], and both reactions (alcohol oxidation reaction at the anode and hydrogen evolution reaction at the cathode) can be performed on low platinum loaded electrodes or platinum-free catalysts [10,11].

Now, the question could be: what is the best alcohol to be used as hydrogen source in an alkaline electrolysis cell. Methanol is the simplest and more reactive alcohol, but it is mainly produced from petrochemical industries and it is a toxic compound. Ethanol is less toxic and is an attractive compound because it can be produced from biomass. But, because the breaking of the C–C bond is very difficult to realize at low temperature, in alkaline medium as well as in acidic one, the main reaction products are acetaldehyde and acetate [12,13] which are non-value added compounds, with only two hydrogen molecules produced from one molecule of ethanol oxidized into acetate. The use of polyols as hydrogen sources can be an interesting alternative. Polyols such as ethylene glycol and glycerol are less toxic than methanol. Each carbon of these compounds carries an alcohol group and as a consequence their partial oxidation without C–C bond breaking and CO_3^{2-} production leads to the simultaneous production of hydrogen and high value added products, with higher amount of hydrogen than in the case of mono-alcohol when oxalate (Eq. (6)), tartronate (Eq. (7)) and mesoxalate (Eq. (8)) are produced:

$$CH_2OH–CH_2OH + 2OH^- \rightarrow COO^–COO^- + 4H_2 \quad (6)$$

$$CH_2OH–CHOH–CH_2OH + 2OH^- \rightarrow COO^–CHOH–COO^- + 4H_2 \quad (7)$$

$$CH_2OH–CHOH–CH_2OH + 2OH^- \rightarrow COO^–CO–COO^- + 5H_2 \quad (8)$$

But again, ethylene glycol is a product from the petrochemical industry, whereas glycerol is a by-product of the biofuel industry which has to be valorised to make this sector profitable. Therefore, the present contribution will focus on glycerol electrooxidation process.

The problem of catalysis is of paramount importance for the selective oxidation of polyols. Palladium is an active material for alcohol electrooxidation in alkaline medium [14], and particularly for glycerol oxidation [15]. It is also known that the modification of palladium by oxophilic metal from the p-group affects dramatically the electrocatalytic behaviour [16], particularly bismuth [17]. But, the role of bismuth in the changes of the catalytic behaviour is not yet really understood. The aim of the present paper is to study the activity and selectivity of Pd nano-catalysts modified by either Bi-adatoms or Bi-clusters toward glycerol electrooxidation. The catalyst composition and structure are indeed very important in electrocatalysis. For example, it has recently been shown on self-supported PdBi materials prepared by a sacrificial support method that the microporous structure of the catalysts influenced its catalytic behaviours, activity as well as selectivity, towards glycerol electrooxidation [18]. The oxidation reactions of alcohols involve several elementary steps: adsorption process, alcohol dehydrogenation reaction, electron transfer, reaction with adsorbed OH and product desorption [19]. And each step can limit the anode performance.

Experimental

Synthesis of catalysts

Non-supported Pd nanoparticles were synthesized according to a method derived from that of Xia and co-workers [20], as follows: 17.4 × 10^{-3} mol of K_2PdCl_4 (Premion® 99.99%, Alfa Aesar) were dissolved in 11 mL of ultrapure water (MilliQ, Millipore, 18.2 MΩ cm) in presence of 87 × 10^{-3} mol of PVP (Polyvinylpyrrolidone, M_w ~ 55,000, Sigma–Aldrich) and reduced by addition of 31 × 10^{-3} mol of L-ascorbic acid (Reagent grade, Sigma–Aldrich). The mixture was heated at 80 °C and the reduction reaction was allowed to proceed for 3 h. After reduction of the palladium salt, the resulting concentrated colloidal solution of Pd nanoparticles was diluted with ultrapure water, and nanoparticles were recovered after removal of the PVP surfactant molecules by addition of NaOH pellets (Semiconductor Grade 99.99%, Aldrich) and precipitation.

Carbon-supported catalysts were prepared via a water-in-oil microemulsion method [17] by mixing $NaBH_4$ (99%, Acros Organics) as reducing agent with a microemulsion carrying the metal salts dissolved in ultrapure water. In particular, K_2PdCl_4, $H_2PtCl_6 \cdot 6H_2O$ and $BiCl_3$ (99.9%, Alfa Aesar) were used. Polyethyleneglycoldodecylether (Brij®30, Fluka) was chosen as surfactant and the organic phase was n-heptane (99%, Acros Organics). Desired amounts of metal salts were dissolved in ultrapure water in order to obtain metallic nanoparticles with controlled compositions. Carbon (Vulcan XC72, Cabot), previously treated under N_2 at 400 °C for 4 h, was added directly in the colloidal solution to obtain the desired metal loading and the mixture was kept under stirring for 2 h. In the present work all supported catalysts were synthesized in order to obtain a 40 wt.% metal loading. The mixture was filtered on a 0.22 μm Durapore® membrane filter (Millipore). The resulting powders were abundantly rinsed with ethanol, acetone and ultrapure water. The carbon-supported catalysts were dried overnight in an oven at 75 °C.

Catalyst characterization

Catalysts were characterized by transmission electron microscopy (TEM) using a JEOL 2100 UHR microscope (200 kV) equipped with a LaB_6 filament. Images were taken with a Gatan Ultrascan 2k × 2k camera. The mean particle sizes and size distributions were determined by measuring the diameters of isolated particles using ImageJ free software [21]. Between 200 and 300 particles were considered for each catalyst in order to have an acceptable statistical sample. The microstructure of the carbon-supported catalysts was evaluated by X-ray diffraction (XRD). The powder diffraction patterns were recorded on a Bruker D5005 Bragg–Brentano (θ-θ) diffractometer operated with a copper tube powered at 40 kV and 40 mA (unfiltered $Cu_{K\alpha 1}$ = 1.542 Å). Measurements were recorded from $\theta = 15°$ to $\theta = 90°$ in step mode, with steps of 0.06° and a fixed acquisition time of 10 s/step. Oxidation states and possible electronic interactions between metals were evaluated by X-ray photoelectron spectroscopy (XPS). Spectra were collected using a VG ESCALAB 3 MKII spectrometer using a monochromatized Mg Kα radiation (1253.6 eV). The source was operated at 300 W (15 kV and 20 mA). Powder analysis covered a surface of 2 mm × 3 mm. XPS spectra were calibrated with respect to the C 1s orbital at 284.6 eV.

Thermogravimetric analyses were carried out with a TA Instrument SDT Q600 apparatus. A few milligrams of catalytic powder was put in an alumina crucible and heated under air from 25 °C to 900 °C. Different temperature slopes were used according to the temperature range: 10 °C min^{-1} from 25 °C to 400 °C, then 2 °C min^{-1} from 400 °C to 600 °C and 10 °C min^{-1} from 600 °C to 900 °C. The catalyst compositions were determined using an inductive coupling plasma optical emission spectrometer (ICP-OES Perkin Elmer Optima 2000 DV).

Electrochemical measurements

Cyclic voltammetry (CV) was conducted using an EG&G PAR model 362 analogue potentiostat that was interfaced with a computer for data acquisition and analysis. All experiments were carried out at room temperature in a classical three-compartment glass electrochemical cell. The solutions were prepared from NaOH (Semiconductor Grade 99.99%, Sigma–Aldrich), glycerol (Reagent Plus ≥ 99%, Sigma–Aldrich) and ultrapure water, deaerated by N_2 bubbling (U-quality, l'Air Liquide). Electrochemical measurements were carried out with a glassy carbon plate as counter electrode (4 cm^2 geometric surface area) and a reversible hydrogen electrode (RHE) as reference electrode, so that all potentials are reported versus RHE.

For non-supported Pd nanoparticles, the working electrode was a gold polished support with a deposit of clean nanoparticles from the suspension previously prepared. A few μL of nanoparticle suspension was put on the gold support using a microsyringe and dried under nitrogen stream. Non-supported Pd nanoparticles were deposited on the clean gold substrate until a greyish deposit was observed.

Carbon-supported catalysts were deposited on a glassy carbon substrate according to a method proposed by Gloaguen et al. [22]. The catalytic powder (25 mg) was added to a mixture of 0.5 mL Nafion® solution (5 wt.% in aliphatic alcohols, Aldrich) in 2.5 mL ultrapure water. After mechanical homogenization of the (catalyst/C)-Nafion® ink, a given volume was deposited from a syringe onto a fresh polished glassy carbon disc (0.071 cm^2 geometric surface area) yielding a catalytic powder loading of ca. 140 μg_{metal} cm^{-2} with 21.85 μg cm^{-2} of Nafion (6 wt.%), leading to a catalytic layer thickness in the range from 1 to 1.5 mm [23,24]. The solvent was then evaporated in a stream of pure nitrogen at room temperature.

In situ FTIR measurements

SPAIRS (Single Potential Alteration IR Spectroscopy), also called LPS-FTIRS (Linear Potential Sweep-FTIRS), experiments were carried out as described elsewhere [25–27]. A Bruker IFS 66v FTIR spectrometer was modified for beam reflection on the electrode surface at a 65° incident angle. To remove interferences from atmospheric water and CO_2 the beam path was vacuum evacuated. An Infrared Associates liquid nitrogen-cooled HgCdTe detector was used. The spectral resolution was 4 cm^{-1} and each spectrum was obtained by

averaging 256 spectra recorded for 35 s. Spectra are recorded each 0.05 V for 35 s during the linear voltammetry carried out at 1 mV s^{-1} from 0.05 V vs. RHE to 1.15 V vs. RHE (i.e. each spectrum represents the average signal recorded on a potential range of 0.035 V).

Results and discussion

Physicochemical characterization

The synthesis of non-supported Pd catalysts leads to spherical nanoparticles with a mean diameter of ca. 4 nm and a narrow size distribution (insets of Fig. 1). The voltammetric profile obtained in alkaline medium with the Pd nanospheres (Fig. 1) showing defined and reversible peaks between 0.25 and 0.55 V in the hydrogen adsorption/desorption region is typical of clean Pd nanoparticle surface. These peaks are related to hydrogen adsorption/desorption on different surface arrangements of Pd atoms [28]. The onset potential of Pd surface oxidation starts just after the hydrogen desorption process, from ca. 0.60 V. The surface of non-supported Pd nanosphere was modified by Bi adatoms by dipping the Pd electrodes into a 0.5 M H_2SO_4 solution saturated by $BiCl_3$ for 0 min, 1 min, 10 min and 30 min, without potential control. The spontaneous adsorption of bismuth is evidenced in the voltammograms of Fig. 2 by the progressive decrease of the charges involved in the hydrogen region and by the increase of the oxidation current at 0.9 V as higher amounts of Bi adatoms are deposited on the Pd surface. The Pd surface coverage increases with the dipping time. After only one minute dipping, the shape of the voltammogram is greatly affected, and the hydrogen desorption feature located as the shoulder at ca. 0.55 V, which is related to hydrogen desorption from {100} surface domains [28], has completely disappeared whereas the feature corresponding to H-desorption from other surface sites (low coordination Pd atoms) remains visible for up to

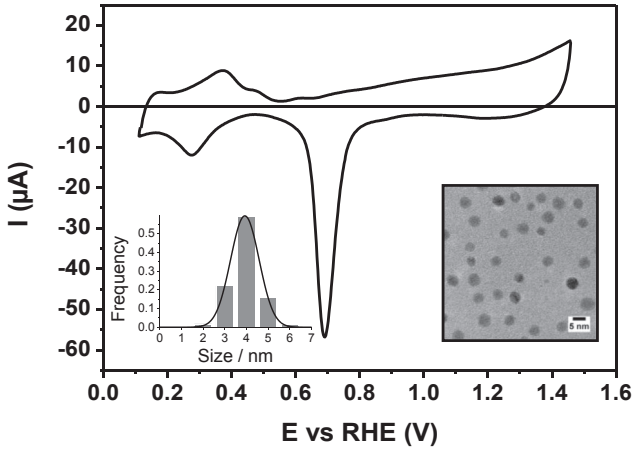

Fig. 1 – Cyclic voltammogram of unsupported Pd nanospheres in N_2-saturated 0.1 M NaOH electrolyte (T = 20 °C, potential scan rate = 5 mV s^{-1}); inset: TEM image of the Pd nanopheres and the corresponding size distribution.

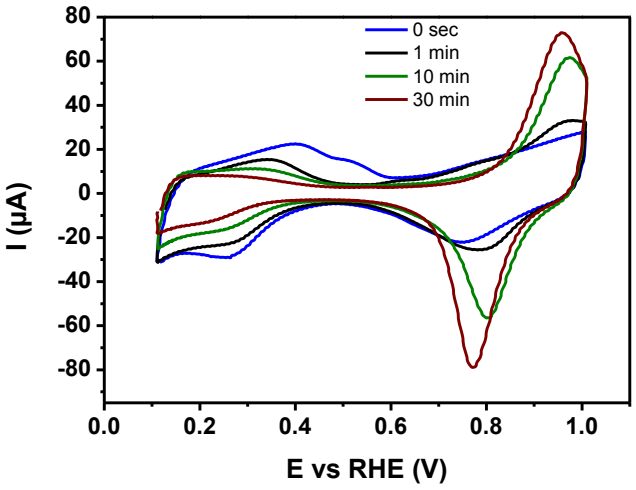

Fig. 2 – Cyclic voltammograms of Bi-modified unsupported palladium nanospheres prepared after dipping in 0.5 M H_2SO_4 solution saturated with $BiCl_3$ for different times (N_2-saturated NaOH 0.1 mol L^{-1}, T = 20 °C, potential scan rate = 20 mV s^{-1}).

30 min dipping. Conversely to the observations made under the same experimental conditions for the spontaneous adsorption of Bi adatoms on Pd nanocubes with high amount of extended {100} surface domains [28], the control of the surface coverage by Bi is made more difficult with nanospheres, probably due to the lack of well-defined surface domains and to the high surface site heterogeneities density (defects, low coordination surface atoms, very small surface domains, etc.). The non-supported Bi-modified Pd catalysts will be further referred as to PdBi, whereas, the carbon-supported catalysts will be further referred as to Pd_xBi_{10-x}/C.

Table 1 reports the main data from the physicochemical characterizations of the carbon-supported catalysts investigated in this work: Pt/C, Pd/C, Pd_xBi_{10-x}/C, Pt_9Bi_1/C and $Pd_{4.5}Pt_{4.5}Bi_1/C$. TGA measurements indicate that metal loadings are close to the nominal ones (40 wt.%). ICP-OES measurements show that the bulk composition of catalysts is also consistent with the nominal ones. Fig. 3 shows typical TEM images of the different considered carbon-supported catalysts and the corresponding size distribution. TEM analyses indicated that the modification by bismuth led to the increase of the mean particle size of palladium based nanomaterials (of ca. 1 nm), from 4.0 nm for Pd/C to ca. 5.0 nm for Pd_xBi_{10-x}/C, whereas it has no significant effect on the mean size of Pt/C based catalysts with metal particle sizes of ca. 5.0 nm for both Pt/C and $Pt_{0.9}Bi_{0.1}/C$ catalysts. The ternary catalyst $Pd_{4.5}Pt_{4.5}Bi_1/C$ displays a mean particle size of ca. 4.5 nm, between those estimated for Pd and Pt monometallic ones. Some zones (Fig. 3(d,f,h)) of Bi-containing catalysts were found to be mainly composed of bismuth species, according to EDX analyses (Fig. 3(k)). XRD patterns in Fig. 4 show that Pd_9Bi_1/C, Pt_9Bi_1/C and $Pd_{4.5}Pt_{4.5}Bi_1/C$ present the typical fcc crystalline structure of palladium, platinum and PtPd alloy, respectively. For higher bismuth content, i.e. for Pd_8Bi_2/C and Pd_7Bi_3/C catalysts, diffraction peaks between $2\theta = 20°$ and $2\theta = 35°$ arise which are assigned to Bi_2O_3 and $Bi(OH)_3$, according to the

Table 1 – Physicochemical characterization of carbon-supported catalysts prepared via the water-in-oil microemulsion method. Metal loading on carbon support from TGA, bulk atomic composition from ICP-OES, surface atomic composition from XPS, cell parameter and Scherrer length from XRD, and particles size from TEM.

	Pd/C	Pd_9Bi_1/C	Pd_8Bi_2/C	Pd_7Bi_3/C	$Pd_{4.5}Pt_{4.5}Bi_1$/C	Pt_9Bi_1/C	Pt/C
wt.% (TGA)	36	38	38	37	38	36	37
at.% (ICP-OES)	100	92/8	84/16	67/33	43/45/12	90/10	100
metal at.% (XPS)	100	84/16	–	54/46	43/40/17	89/11	100
Cell parameter/Å	0.3938	0.3938	0.3939	0.3958	0.3943	0.3943	0.3942
Sherrer length/Å	4.1	4.5	–	–	4.7	5.7	5.5
Particle size/nm	4.0	5.2	4.9	5.2	4.5	4.7	5.3

JCPDS cards n° 071-0465 and n° 001-0898, respectively. These diffraction peaks point out the presence of unalloyed bismuth oxide species (Bi_2O_3 and $Bi(OH)_3$ clusters most probably isolated from palladium particles). XPS measurements also indicated the presence of Bi_2O_3 and $Bi(OH)_3$ species, as well as interaction between Pd or Pt and Bi [17,29]. The bismuth concentration determined by XPS was always higher than that of bulk composition determined by ICP-OES or nano EDX, indicating a Bi-enrichment of the catalyst surface. It has then been proposed that bismuth in interaction with Pd or Pt was localised on the surface of platinum or palladium particles [17]. Voltammograms recorded in supporting electrolyte are presented in Fig. 5. In the cases of Pd_xBi_{10-x}/C, the presence of bismuth inhibits the adsorption/desorption reaction of hydrogen on palladium. Casella and Contursi [30] verified a similar effect on palladium electrodes modified by bismuth adatoms. Considering the Pt_9Bi_1/C catalyst, an oxidation current starts to appear from ca. 0.7 V vs RHE which is related to the palladium surface oxidation [31]:

$$Pd + 2OH^- \rightarrow PdO + H_2O + 2e^- \quad (9)$$

Then, an intense oxidation peak located at ca. 0.9–0.95 V vs RHE was assigned to surface oxidation processes of bismuth. According to the potential-pH diagram of bismuth [32] in aqueous medium, the Bi_2O_3 bismuth oxide phase exists under its hydrated form $Bi(OH)_3$, which is insoluble in alkaline solutions. As referred by the author, bismuth oxidation in aqueous media may start from 0.48 V according to the following reaction Eq. (10):

$$2Bi + 6OH^- \rightarrow 2Bi(OH)_3 + 6e^- \quad (10)$$

In the negative-going potential scan, the reduction current peak at ca. 0.7 V is attributed to simultaneous reduction of palladium and bismuth surface oxides [30] formed during the positive-going potential scan. This fact suggests that bismuth redox process is related to the palladium redox one confirming the electronic interaction between both metals, as shown by XPS measurements. In the case of Pd_8Bi_2/C and Pd_7Bi_3/C catalysts, in addition to this redox process, oxidation/reduction peaks occur at lower potentials, which are related to redox processes involving Bi species deposited on the carbon support (as shown by TEM images in Fig. 3(d) and (f) and by the peaks between 20° and 35° in the diffraction pattern of the Pd_7Bi_3/C catalyst in Fig. 4) or having weaker interactions with Pd particles.

In the case of the carbon-supported Pt_9Bi_1/C sample the presence of bismuth leads again to inhibit the adsorption reaction of hydrogen on platinum. Two quasi-reversible oxidation/reduction peaks are visible in the voltammogram of Pt_9Bi_1/C at ca. 0.75 V and 0.95 V vs RHE. The first peak at 0.75 V was previously attributed to the oxidation of bismuth disseminated on the carbon surface, whereas the peak at higher potential was assigned to the oxidation of bismuth at the platinum surface [29]. The voltammogram of $Pd_{4.5}Pt_{4.5}Bi_1$/C in alkaline medium shows that the surface oxidation follows the same mechanism as that proposed for the Pt_9Bi_1/C material. For all catalysts modified by bismuth the negative-going scan led to a reduction peak located at the same potentials for the reduction of Pt, Pd or PdPt materials, but much more intense, which was assigned to the simultaneous reduction of noble metal and Bi oxides [30], clearly indicating electronic interaction between both metals.

Glycerol electrooxidation

The electrooxidation of glycerol was evaluated on non-supported Pd nanospheres in 0.1 M glycerol + 0.1 M NaOH solution (Fig. 6). First, it can be seen that the Pd nanosphere surface has undergone some structural changes between the first and the third cycles, as the glycerol electrooxidation pre-wave from ca. 0.6 V to ca. 0.85 V has decreased with the number of cycles. For further cycling after this electrode activation process, no change was observed in the glycerol oxidation voltammograms (not shown). In a previous work, this oxidation pre-wave was found more intense in the case of Pd nanocubes with high amount of {100} surface nanodomains [28], and was then assigned to glycerol adsorption and oxidation on such surface domains. After several cycles with the upper potential limit in the region of Pd surface oxide formation, it is likely that the {100} surface domains are destroyed, as it is the case for Pt nanoparticles with preferentially oriented surface domains [33], leading to lower activity at lower overpotentials. The modification of the surface after 30 min dipping in the 0.5 M H_2SO_4 solution saturated by $BiCl_3$ leads to high Pd surface coverage, ca. 90%, and to the highest activity [28]. The modification of the non-supported Pd nanoparticles by bismuth adatoms leads to an increase of the activity towards glycerol electrooxidation. It is worth to note that the activity of the pure non-supported Pd catalyst decreases from the first cycle to the third one, particularly in the low overpotential region from ca. 0.6 V to ca. 0.9 V, whereas that obtained with the Bi-modified one remains constant in the low overpotential region and increases in the high

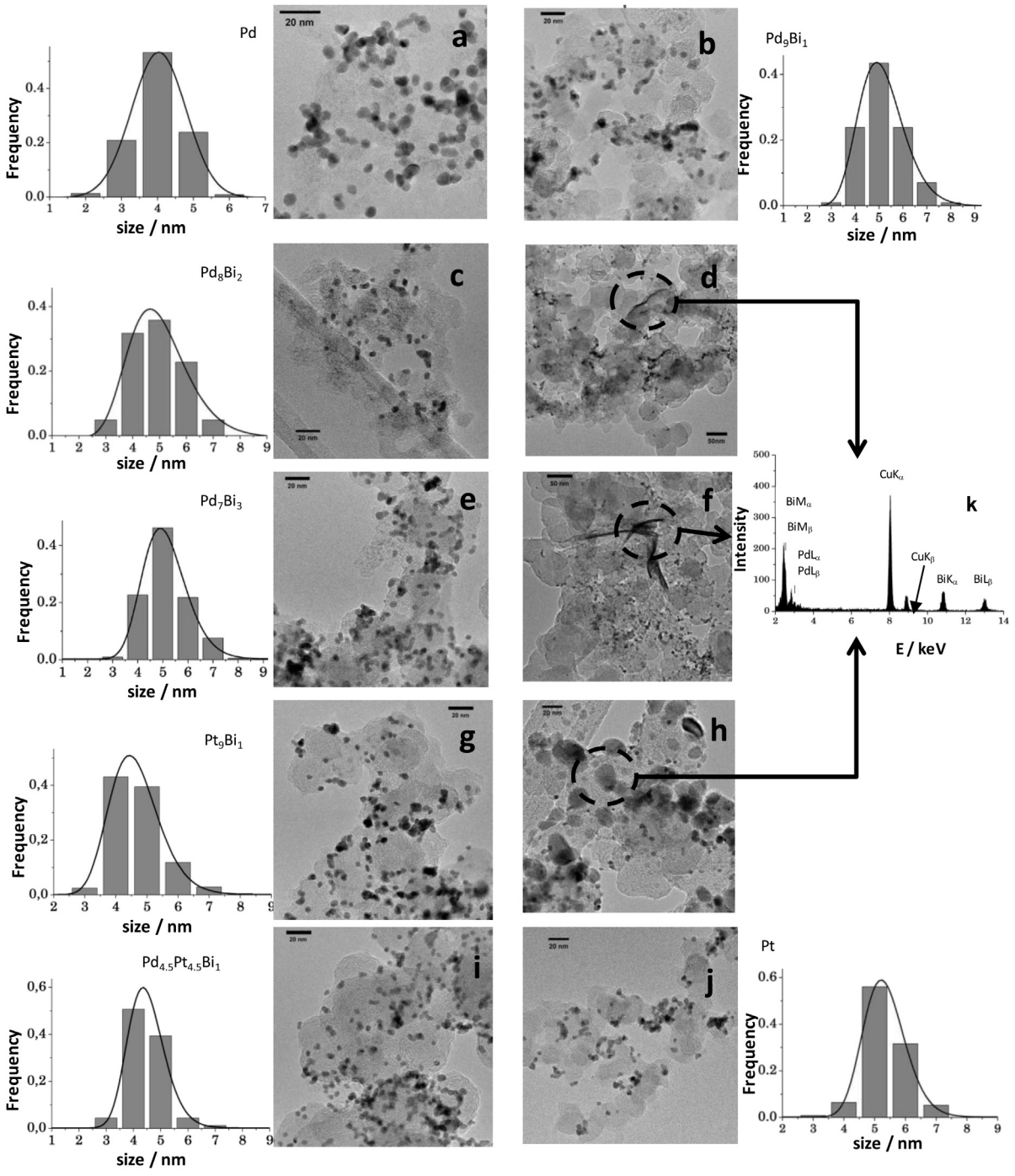

Fig. 3 – TEM pictures and size distribution for the different carbon-supported catalysts (40 wt.% metal loading on carbon) prepared via the water-in-oil microemulsion method. (a) Pd/C, (b) Pd_9Bi_1/C, (c) and (d) Pd_8Bi_2/C, (e) and (f) Pd_7Bi_3/C, (g) and (h) Pt_9Bi_1/C, (i) $Pd_{4.5}Pt_{4.5}Bi_1$/C and (j) Pt/C. TEM images (d), (f) and (h) show bismuth-based structures on Pd_8Bi_2/C, Pd_7Bi_3/C and Pt_9Bi_1/C, respectively, as identified by (k) nano EDX measurements.

potential region. However, the effect of bismuth on the activity towards glycerol electrooxidation is not as high as expected.

Indeed, in the case of carbon-supported Pd_xBi_{10-x}/C catalysts prepared by the water-in-oil microemulsion method, a dramatic effect of bismuth towards glycerol electrooxidation activity was observed (Fig. 7(a)). The addition of 10 at.% of bismuth to palladium leads to the same activity as that obtained with a Pt/C catalyst, which is a very remarkable result. The onset potential is shifted by ca. 150 mV towards lower potentials, from ca. 0.55 V to ca. 0.40 V. Note that the increase of the Bi atomic ratio has no effect on the activity, which confirms that extra bismuth atoms are deposited on the carbon support and does not play any catalytic role. The

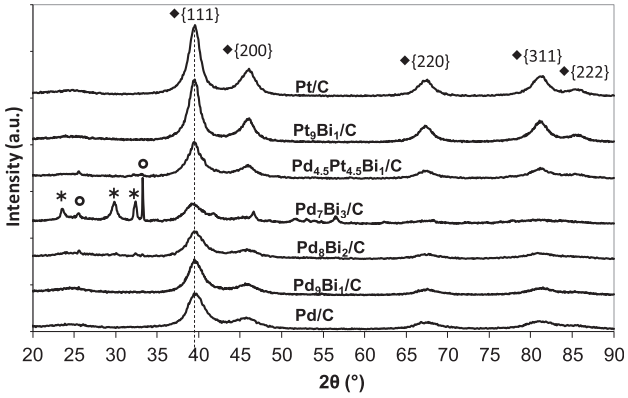

Fig. 4 – XRD diffraction patterns of the different carbon-supported catalysts (40 wt.% metal loading on carbon). ◆ Pd diffraction peaks, ∗ Bi_2O_3 diffraction peaks and ○ $Bi(OH)_3$ diffraction peaks.

discrepancy between the results obtained with non-supported Pd nanospheres modified by spontaneous adsorption of bismuth adatoms and with the carbon-supported Pd_xBi_{10-x}/C nanospheres are certainly due to the nature/structure of the Bi deposits and to their interaction with palladium surface, as both kinds of Pd nanoparticles are spherical with same size, ca. 4.0 nm.

In the case of the irreversible adsorption of Bi on Pd surfaces, the very low amount of deposited bismuth atoms at the Pd particle surface made difficult the determination of the Bi valence and of the nature of the Bi deposit. Clavilier et al. [34] proposed a zero valence for spontaneously adsorbed Bi. Hamm et al. [35] also proposed a 0 valence adsorbed Bi at Pt {111} surface on both sides of the UPD peak. On gold surface, Gewirth et al. found that Bi–OH and Bi–O species were formed in the catalytically active region and that OH^- was co-adsorbed with Bi in the UPD region [36,37]. But recently, Cai et al. [38] demonstrated on the basis of XPS studies that Bi(III) was the prominent valence of Bi atoms deposited via the same irreversible adsorption method as that used in the present work. Furthermore, it is generally proposed that the role of Bi, either deposited spontaneously or by UPD method, is to favour the adsorption of OH species, either on its surface [34] or on adjacent noble metal sites [39]. In the case of supported Pd_xBi_{10-x}/C catalysts, TEM, XRD and XPS characterizations, together with cyclic voltammetry measurements, suggested that Pd nanoparticles were decorated by Bi_2O_3, or more likely $Bi(OH)_3$ clusters in an aqueous alkaline environment.

Now, looking at the CVs of glycerol electrooxidation, the modification of palladium by bismuth does not affect the general shape whatever the catalyst preparation method is, it only leads to increase the current over the whole potential range where palladium is active. No additional oxidation peaks appears, which seems to indicate that no change in the reaction pathway (and in the selectivity) is involved by the presence of bismuth. This was confirmed by *in situ* infrared spectroscopy measurements during glycerol electrooxidation on a Pd_9Bi_1/C catalyst (Fig. 8(a)), where the absorption peaks located at 1310 cm^{-1}, 1385 cm^{-1} and 1570 cm^{-1} are assigned to the formation of glycerate ions [15], as for Pd alone. The only

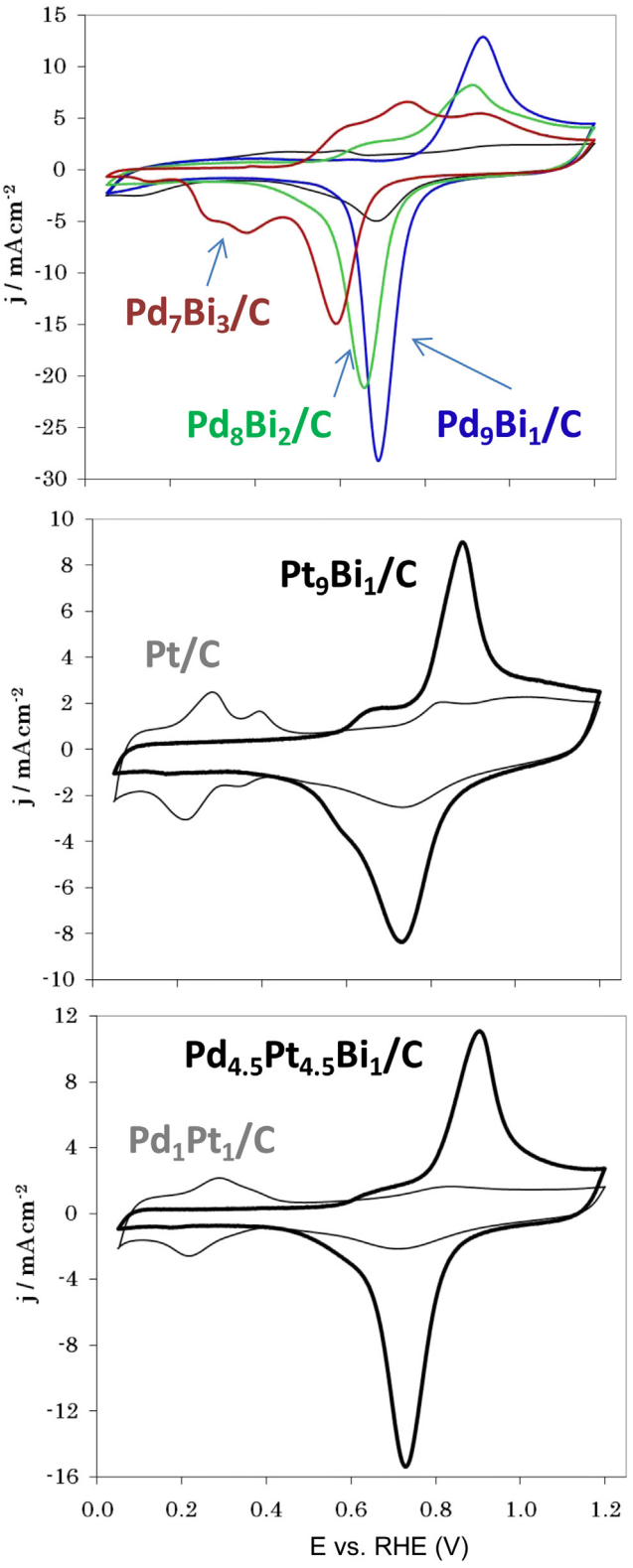

Fig. 5 – Cyclic voltammograms of carbon-supported catalysts prepared via the water-in-oil microemulsion method. (a) Pd_xBi_{10-x}/C catalysts, (b) Pt/C (black line) and Pt_9Bi_1/C (grey line) catalysts and (c) Pt_1Pd_1/C (black line) and $Pd_{4.5}Pt_{4.5}Bi_1/C$ (grey line); $v = 50$ mV s^{-1}, N_2-saturated 1 mol L^{-1} NaOH electrolyte, $T = 20$ °C.

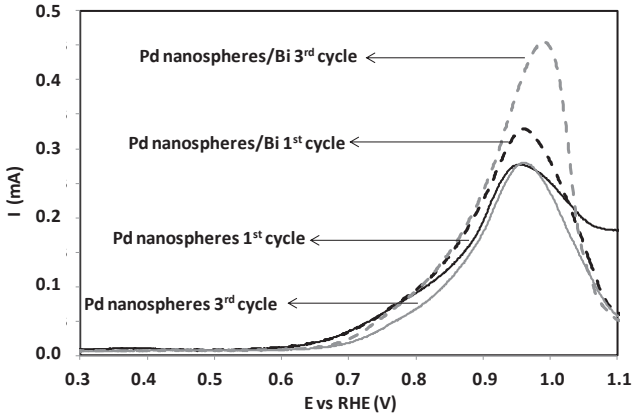

Fig. 6 – Polarization curves of glycerol oxidation recorded on non-supported Pd nanospheres and Bi-modified by spontaneous adsorption non-supported Pd nanospheres (with the maximum coverage of Pd surface by Bi-adatoms) in a N_2-saturated 0.1 mol L^{-1} NaOH solution (T = 20 °C, scan rate = 5 mV s^{-1}).

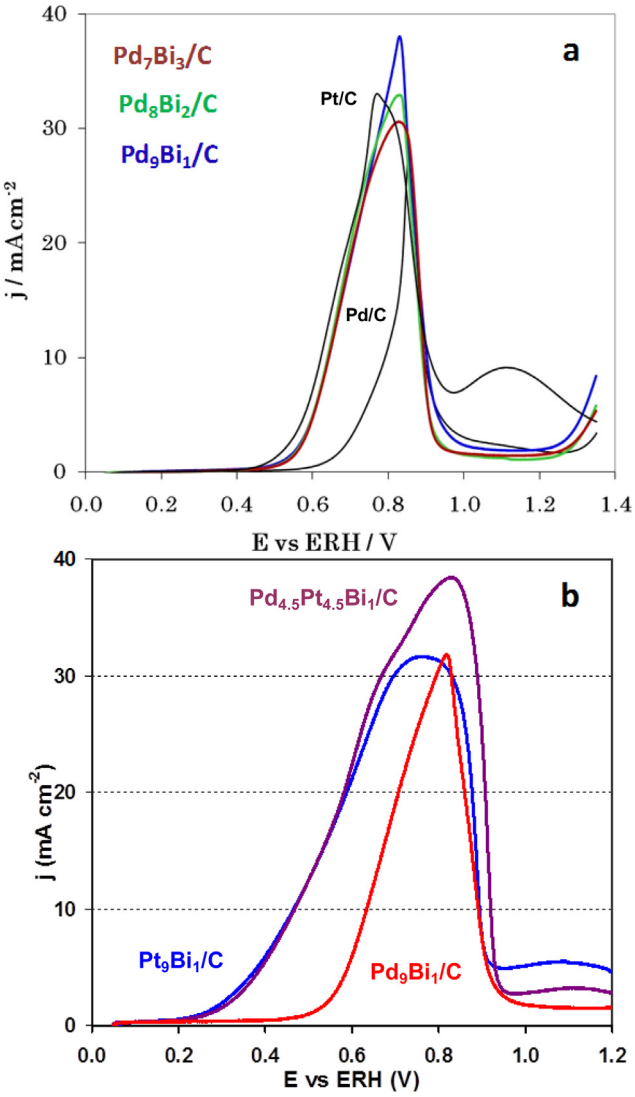

Fig. 7 – Polarization curves of glycerol oxidation recorded on carbon-supported catalysts prepared by the water-in-oil microemulsion method. (a) Pt/C, Pd/C, Pd_xBi_{10-x}/C and (b) Pd_9Bi_1/C, Pt_9Bi_1/C and $Pd_{4.5}Pt_{4.5}Bi_1$/C; v = 10 mV s^{-1}, N_2-saturated, 0.1 mol L^{-1} glycerol + 1.0 mol L^{-1} NaOH electrolyte, T = 20 °C.

difference is that these peaks appeared at lower potentials than in the case of pure Pd/C catalyst (not shown), due to the presence of bismuth. However, with platinum (in the cases of the binary Pt_9Bi_1/C and ternary $Pd_{4.5}Pt_{4.5}Bi_1$/C catalysts) the addition of bismuth results in an important shift of the glycerol oxidation onset potential down to 0.2 V (Fig. 7(b)), which is accompanied with a high selectivity into dihydroxyacetone (absorption band at ca. 1335 cm^{-1}) and glyceraldehydes (absorption band at ca. 1225 cm^{-1}) at low potentials from 0.25 to 0.60 V vs. RHE (Fig. 8(b) and (c)). In these both later cases, the electrode potential is likely too low to allow activating water molecules or hydroxyl ions, preventing the over-oxidation of glycerol into carboxylate species conversely to what happens with palladium. The enhancement of activity in this potential range could then not be explained in terms of the bifunctional mechanism [40], where desorption of organic poisoning species involves H_2O activation and reaction with adsorbed species, but in terms of electronic effect and/or glycerol adsorption mode controlling the selectivity towards ketone or aldehyde species.

Conclusion

The Modification of Pd and/or Pt catalysts by bismuth has obviously an effect on the activity of the catalytic material towards glycerol oxidation. However, the method of modification by bismuth implies different catalytic behaviours: on non-supported Pd nanoparticles, Bi adatoms leads to relatively limited improvement of Pd nanospheres activity towards glycerol electrooxidation, whereas on carbon-supported Pd_xBi_{10-x}/C, Pt_9Bi_1/C and $Pd_{4.5}Pt_{4.5}Bi_1$/C catalysts, very high enhancement of the catalytic activity is observed. The nature of the Bi deposited (adatoms, oxides, hydroxydes) at the surface of the catalytic metal, and the microstructure of the catalyst, are responsible of such a discrepancy. In order to better understand the role of palladium surface and bismuth modification on polyol oxidation, further works will be carried out on Pd nanocubes and nanooctahedrons with high amount of {100} and {111} surface nanodomains, respectively, and nanospheres without preferential surface orientation. Glycerol electrooxidation will be studied and compared on both nanoparticles, before and after modification by adatoms; *in situ* infrared spectroscopy measurements of glycerol electrooxidation on Bi-modified Pd surfaces will be performed to determine adsorbed intermediates versus Bi surface coverage. Spectroscopic studies will be completed by HPLC determination of the reaction product distribution after chronoamperometry measurements for determining the reaction mechanisms and the role of Bi.

At last, a high selectivity towards aldehydic or ketonic compounds is obtained at very low potential with Pt

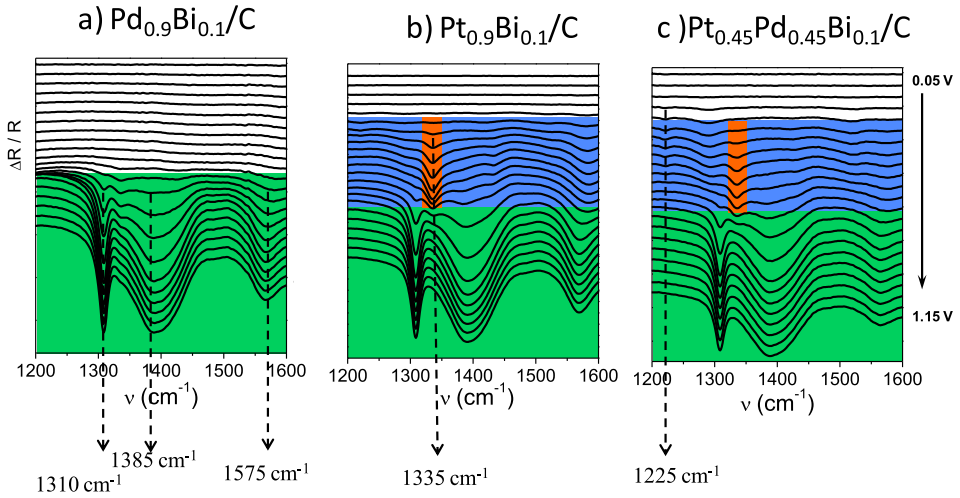

Fig. 8 – Infrared spectra recorded during glycerol oxidation on carbon-supported catalysts prepared by the water-in-oil microemulsion method. (a) Pd_9Bi_1/C, (b) Pt_9Bi_1/C, and (c) $Pd_{4.5}Pt_{4.5}Bi_1$/C catalysts in 0.1 mol L^{-1} glycerol, 1.0 mol L^{-1} NaOH electrolyte at 20 °C. Scan rate: 1 mV s^{-1}, resolution 4 cm^{-1}.

containing catalyst, whereas the onset potential for glycerol electrooxidation at Pd_xBi_{10-x}/C catalysts remains too high and favours the formation of carboxylate. At low potentials, the oxidation of glycerol occurs without activation of OH species allowing the formation of aldehyde and ketone groups. The formation of carboxylate groups appears at higher potential, leading to two potential domains with an important difference of selectivity.

REFERENCES

[1] Ioroi T, Fujiwara N, Siroma Z, Yasuda K, Miyazaki Y. Platinum and molybdenum oxide deposited carbon electrocatalyst for oxidation of hydrogen containing carbon monoxide. Electrochem Commun 2002;4:442–6.

[2] Millet P, Andolfatto F, Durand R. Design and performance of a solid polymer electrolyte water electrolyzer. Int J Hydrogen Energy 1996;21:87–93.

[3] Marshall A. Characterisation of electrocatalysis for water electrolysis. Trondheim, Norway: NTNU; 2005. pp. 1–233. PhD thesis.

[4] Grigoriev S, Porembsky V, Fateev V. Pure hydrogen production by PEM electrolysis for hydrogen energy. Int J Hydrogen Energy 2006;31:171–5.

[5] Marshall A, Sunde S, Tsypkin M, Tunold R. Performance of a PEM water electrolysis cell using $Ir_xRu_yTa_zO_2$ electrocatalysts for the oxygen evolution electrode. Int J Hydrogen Energy 2007;32:2320–4.

[6] Lamy C, Devadas A, Simoes M, Coutanceau C. Clean hydrogen generation through the electrocatalytic oxidation of formic acid in a proton exchange membrane electrolysis cell (PEMEC). Electrochim Acta 2012;60:112–20.

[7] Lamy C, Jaubert T, Baranton S, Coutanceau C. Clean hydrogen generation through the electrocatalytic oxidation of ethanol in a proton exchange membrane electrolysis cell (PEMEC): effect of the nature and structure of the catalytic anode. J Power Sources 2014;245:927–36.

[8] Simoes M, Baranton S, coutanceau C. Electrochemical valorization of glycerol. ChemSusChem 2012;5:2106–24.

[9] Yang CC. Preparation and characterization of electrochemical properties of air cathode electrode. Int J Hydrogen Energy 2004;29:135–43.

[10] Marozzi CA, Chialvo AC. Development of electrode morphologies of interest in electrocatalysis: part 2: hydrogen evolution reaction on macroporous nickel electrodes. Electrochim Acta 2001;46:861–6.

[11] Baranton S, Coutanceau C. Nickel cobalt hydroxide nanoflakes as catalysts for the hydrogen evolution reaction. Appl Catal B Environ 2013;136–137:1–8.

[12] Rousseau S, Coutanceau C, Lamy C, Léger JM. Direct ethanol fuel cell (DEFC): electrical performances and reaction products distribution under operating conditions with different platinum-based anodes. J Power Sources 2006;158:18–24.

[13] Bambagioni V, Bianchini C, Marchionni A, Filippi J, Vizza F, Teddy J, et al. Pd and Pt–Ru anode electrocatalysts supported on multi-walled carbon nanotubes and their use in passive and active direct alcohol fuel cells with an anion-exchange membrane (alcohol = methanol, ethanol, glycerol). J Power Sources 2009;190:241–51.

[14] Bianchini C, Shen PK. Palladium-based electrocatalysts for alcohol oxidation in half cells and in direct alcohol fuel cells. Chem Rev 2009;109:4183–206.

[15] Simoes M, Baranton S, Coutanceau C. Electro-oxidation of glycerol at Pd based nano-catalysts for an application in alkaline fuel cells for chemicals and energy cogeneration. Appl Catal B Environ 2010;93:354–62.

[16] Serov A, Martinez U, Atanassov P. Novel Pd–In catalysts for alcohols electrooxidation in alkaline media. Electrochem Commun 2013;34:185–8.

[17] Simoes M, Baranton S, Coutanceau C. Enhancement of catalytic properties for glycerol electrooxidation on Pt and Pd nanoparticles induced by Bi surface modification. Appl Catal B Environ 2011;110:40–9.

[18] Zalineeva A, Serov A, Padilla M, Martinez U, Artyushkova K, Baranton S, et al. Self-supported Pd_xBi catalysts for the electrooxidation of glycerol in alkaline media. J Am Chem Soc 2014;136:3937–45.

[19] Vigier F, Rousseau S, Coutanceau C, Léger JM, Lamy C. Electrocatalysis for the direct alcohol fuel cell. Top Catal 2006;40:111–21.

[20] Lim B, Jiang MJ, Tao J, Camargo PHC, Zhu YM, Xia YN. Shape-controlled synthesis of Pd nanocrystals in aqueous solutions. Adv Funct Mater 2009;19:189–200.
[21] Rasband WS, Image J, US National Institutes of Health, Bethesda, MA, USA, http://rsbweb.nih.gov/ij/.
[22] Gloaguen F, Andolfatto N, Durand R, Ozil P. Kinetic study of electrochemical reactions at catalyst-recast ionomer interfaces from thin active layer modelling. J Appl Electrochem 1994;24:863–9.
[23] Molina Concha B, Chatenet M. Direct oxidation of sodium borohydride on Pt, Ag and alloyed Pt–Ag electrodes in basic media: Part II. Carbon-supported nanoparticles. Electrochim Acta 2009;54:6130–9.
[24] Yano H, Iguchi E, Uchida H, Watanabe M. Temperature dependence of oxygen reduction activity at Nafion-coated bulk Pt and Pt/carbon black catalysts. J Phys Chem B 2006;110:16544–9.
[25] Beden B, Lamy C. Infrared reflectance spectroscopy. In: Gale RJ, editor. Spectroelectrochemistry, theory and practice. New York: Plenum Press; 1988. pp. 189–261.
[26] Kabbabi A, Faure R, Durand R, Beden B, Hahn F, Léger JM, et al. In situ FTIRS study of the electrocatalytic oxidation of carbon monoxide and methanol at platinum–ruthenium bulk alloy electrodes. J Electroanal Chem 1998;444:41–53.
[27] El Chbihi M, Takky D, Hahn F, Huser H, Léger JM, Lamy C. In-situ infrared reflectance spectroscopic study of propanediol electrooxidation at platinum and gold: part 1. 1,3-Propanediol. J Electroanal Chem 1999;463:63–71.
[28] Zalineeva A, Baranton S, Coutanceau C. Bi-modified palladium nanocubes for glycerol electrooxidation. Electrochem Commun 2013;34:335–8.
[29] Simoes M, Baranton S, Coutanceau C. Influence of bismuth on the structure and activity of Pt and Pd nanocatalysts for the direct electrooxidation of $NaBH_4$. Electrochim Acta 2010;56:580–91.
[30] Casella IG, Contursi M. Characterization of bismuth adatom-modified palladium electrodes: the electrocatalytic oxidation of aliphatic aldehydes in alkaline solutions. Electrochim Acta 2006;52:649–57.
[31] Grdeń M, Łukaszewski M, Jerkiewicz G, Czerwiński A. Electrochemical behaviour of palladium electrode: oxidation, electrodissolution and ionic adsorption. Electrochim Acta 2008;53:7583–98.
[32] Van Muylder J, Pourbaix M. Atlas d'équilibres électrochimiques à 25 °C. Paris: Gauthier-Villars & Cie; 1963.
[33] Urchaga P, Baranton S, Coutanceau C. Changes in CO_{chem} oxidative stripping activity induced by reconstruction of Pt (111) and (100) surface nanodomains. Electrochim Acta 2013;92:438–45.
[34] Clavilier J, Feliu JM, Aldaz A. An irreversible structure sensitive adsorption step in bismuth underpotential deposition at platinum electrodes. J Electroanal Chem 1988;243:419–33.
[35] Hamm UW, Kramer D, Zhai RS, Kolb DM. On the valence state of bismuth adsorbed on a Pt(111) electrode: an electrochemistry, LEED and XPS study. Electrochim Acta 1988;43:2969–78.
[36] Niece BK, Gewirth AA. Potential-step chronocoulometric investigation of the surface coverages of coadsorbed Bi and hydroxide on Au(111) electrodes. Langmuir 1996;12:4909–13.
[37] Li X, Gewirth AA. Peroxide electroreduction on Bi-modified Au surfaces: vibrational spectroscopy and density functional calculations. J Am Chem Soc 2003;125:7086–99.
[38] Cai J, Huang Y, Guo Y. Bi-modified Pd/C catalyst via irreversible adsorption and its catalytic activity for ethanol oxidation in alkaline medium. Electrochim Acta 2013;99:22–9.
[39] Schmidt TJ, Behm RJ, Grgur BN, Markovic NM, Ross Jr PN. Formic acid oxidation on pure and Bi-modified Pt(111): temperature effects. Langmuir 2000;16:8159–66.
[40] Watanabe M, Motoo S. Electrocatalysis by ad-atoms: part III. Enhancement of the oxidation of carbon monoxide on platinum by ruthenium ad-atoms. J Electroanal Chem 1975;60:275–83.